Plasmonic spectral splitting in multi-resonator-coupled waveguide systems

Chao Zeng

State Key Laboratory of Transient Optics and Photonics, Xi'an Institute of Optics and Precision Mechanics, Chinese Academy of Sciences, Xi'an 710119, China (zengchao@opt.cn)

Received 8 October 2013; accepted 15 November 2013;
posted 2 December 2013 (Doc. ID 198777); published 23 December 2013

Spectral splitting is numerically investigated in a metal-insulator-metal plasmonic waveguide coupled with a series of disk cavities for the first time to our best knowledge. The finite-difference time-domain simulations find that, when an identical cavity is introduced into the single-cavity-coupled structure, a resonance peak emerges in reflection dip due to the plasmonic analogue of electromagnetically induced transparency. By cascading multiple cavities into the waveguide system, the resonance spectra are gradually split because of the phase-coupled effects. Particularly, the quality factors of splitting resonance spectra can be rapidly improved with increasing the number of coupled cavities. The proposed plasmonic systems may find potential applications in highly integrated optical circuits, especially for multichannel filtering, all-optical switching, and slow-light devices.

OCIS codes: (240.6680) Surface plasmons; (230.4555) Coupled resonators; (060.4230) Multiplexing; (130.3120) Integrated optics devices.
http://dx.doi.org/10.1364/AO.53.000038

1. Introduction

Surface plasmon polaritons (SPPs) are waves propagating along the metal-dielectric interface due to the interaction between the light waves and the free electrons of the conductor [1]. A considerable amount of research has been carried out on SPPs owing to their capability to overcome the diffraction limit and local field enhancement, making it possible that minimizing high-integrated optical devices and manipulating photons efficiently at nanoscales [2]. To date, numerous fascinating phenomena based on SPPs have been theoretically predicted and experimentally demonstrated [3–8]. For instance, Wang *et al.* proposed the graded grating and tapered waveguides with the well confinement of SPPs to realize the trapping of light [9,10]. Verellen *et al.* presented an experimental demonstration of Fano resonances in the individual coherent plasmonic nanocavities [11]. Chen *et al.* experimentally realized an optical response in a dielectric-film-coated asymmetric T-shape single slit based on the analogue of electromagnetically induced transparency (EIT) [12]. Moreover, various types of plasmonic devices have been proposed, such as plasmonic reflectors [13,14], demultiplexers [15–18], Bragg gratings [19], absorbers [20], couplers [21], filters [22–26], switching [27–30], and lenses [31].

As an intriguing physical phenomenon, EIT features a narrow transparency resonance in the broad absorption spectrum and extremely strong dispersion, originating from the quantum-interference-induced elimination of absorption in a coherently driven atomic system [32]. Recently, extensive attention has been paid to the realization of the EIT-like effects in plasmonic systems due to the tremendous optical properties and applications [33–35]. The coupled optical-resonator systems can give rise to the EIT-like responses through the coherent interference of coupled resonators, known as the coupled-resonator induced transparency [36–38]. Lu *et al.* theoretically and numerically studied the spectral control, slow-light effects, and optical bistability in nanoscale waveguide-resonator systems on the basis

1559-128X/14/010038-06$15.00/0

of EIT [36,37,39,40]. The plasmonic resonator systems also can realize multiple EIT-like responses, which is valuable and desirable for the manipulation of light in plasmonic nanostructures [36,37,41,42].

In this paper, the spectral splitting behaviors are numerically investigated in the compact plasmonic structure consisting of a metal-insulator-metal (MIM) waveguide coupled with a series of disk cavities. By using the finite-difference time-domain (FDTD) simulations, it is found that the reflection spectra can be effectively split through cascading multiple cavities into the waveguide system. Note that the quality factors of splitting resonance spectra exhibit rapid improvements and can approach the level of several hundreds due to the spectral splitting. The proposed plasmonic systems may find potential applications for low-threshold optical switching and high group-index slow-light devices.

2. Structure Model

Figure 1 depicts the cross-section schematic diagram of our plasmonic structure. It consists of a MIM waveguide coupled with a central disk nanocavity and a series of side-coupled identical cavities. The proposed structure is symmetrical with reference to the waveguide. r and w are the cavity radius and waveguide width, respectively. d represents the coupling distance between waveguide and central cavity, and g is the coupling distance between adjacent cavities. When a transverse-magnetic wave is injected into the waveguide, SPP waves are excited on the metallic interfaces and confined in the MIM plasmonic structure [7,9,10]. The insulators in the waveguides and cavities are assumed as air. The metal is selected as silver, whose frequency-dependent relative permittivity can be characterized by the Drude model [19,24,43]:

$$\varepsilon_m(\omega) = \varepsilon_\infty - \frac{\omega_p^2}{\omega(\omega + i\gamma)}.$$

Here ε_∞ stands for the dielectric constant at the infinite frequency; ω_p and γ are bulk plasma frequency of free conduction electrons and damping frequency of the electron oscillations, respectively. ω represents the angular frequency of incident light. These parameters for silver are chosen as $\varepsilon_\infty = 3.7$, $\omega_p = 9.1$ eV, and $\gamma = 0.018$ eV [19,39]. The FDTD method is utilized to investigate the spectral responses of the proposed waveguide systems. A 2D model, as illustrated in Fig. 1, is constructed by setting a periodic boundary condition in the z direction. In the FDTD algorithm, the spatial and temporal calculation steps are set as $\Delta x = \Delta y = 5$ nm and $\Delta t = \Delta x/2c$, respectively. The perfectly matched layers are employed to absorb outgoing waves from the computation domain [42].

3. Results and Discussion

The waveguide width w and coupling distance d between waveguide and central cavity are fixed at 50 and 20 nm, respectively. Figure 2(a) illustrates the reflection spectra of the plasmonic waveguide coupled with single- and dual-disk cavities. It is found that the reflection spectrum exhibits a reflection dip with the single central cavity, which results from the coupling resonance effects [25,26]. When another identical cavity (i.e., cavity 2) is introduced into the resonator waveguide structure, a reflection peak at the central wavelength of 554 nm is generated in the original broad dip, as shown in Fig. 2(a). The resonance spectrum exhibits an EIT-like response in the plasmonic system [35]. To verify this, the field distributions at the resonance wavelengths are plotted in Figs. 2(c) and 2(d). It can be seen that the resonance mode at the wavelength of 554 nm is established in the single central cavity, which is prohibited in the dual-cavity-coupled structure. The results can be explained via the EIT-like behavior: the destructive interference between the two optical excitation pathways, namely, the direct excitation of plasmonic mode in the central cavity by the external light and the excitation by coupling with the side-coupled cavity [40]. Figure 2(b) shows the enhancement of reflectance when a triple-cavity-coupled structure is constructed by adding another identical cavity (i.e., cavity 3) at the other side of the central cavity. The maximum enhancement of reflectance approaches ~18%. It is found that the reflectance of resonance peaks decreases with the increase of

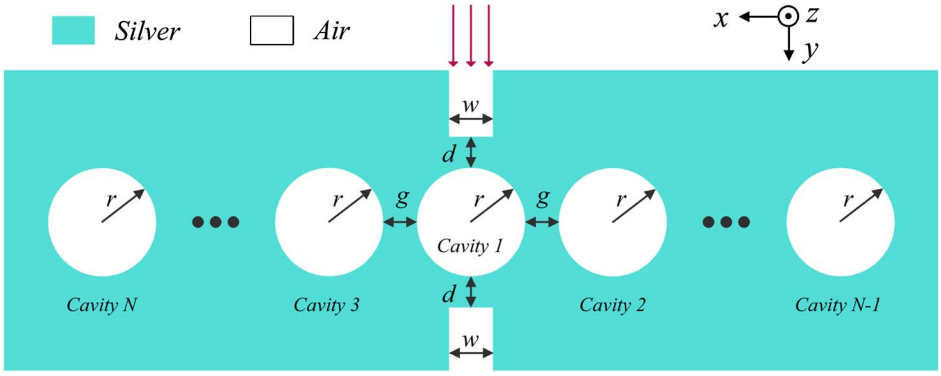

Fig. 1. Schematic diagram of the multi-resonator-coupled plasmonic system. r: radius of nanocavity resonator; w: width of the waveguide; d: coupling distance between the waveguide and central cavity; g: coupling distance between adjacent cavities. N is an odd number.

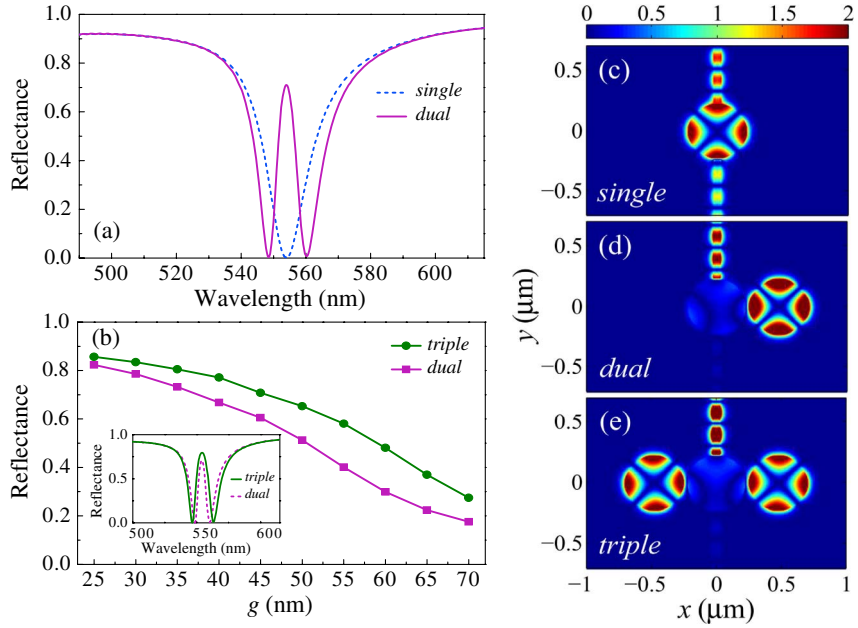

Fig. 2. (a) Reflection spectra in the plasmonic waveguide system with single- and dual-coupled cavities. (b) Reflectance versus the cavity-cavity coupling distance g with dual- and triple-coupled cavities. The inset shows the reflection spectra for $g = 38$ nm. (c)–(e) Field distributions ($|H_z|$) at the wavelength of 554 nm in the single-, dual-, and triple- (Media 1) cavity coupled structures. The geometrical parameters are set as $r = 220$ nm and $g = 38$ nm.

the cavity-cavity coupling distance g, while the enhancement increases. The field distribution in Fig. 2(e) at the reflection peak reveals that the two side-coupled cavities simultaneously induce the generation of EIT-like resonance and also enhance the resonance spectrum. To obtain more obvious spectral responses, we mainly focus on the symmetrical multicavity-coupled waveguide structure. The resonance wavelength is strongly dependent on the radius of cavity, which enables the tunability of the EIT window [25,26]. As shown in Fig. 3, the spectral peak displays a red-shift with the increase of cavity radius.

Note that the spectral splitting of the EIT-like resonance peak occurs when a pair of cavities are arranged to couple with the symmetrical triple-cavity-coupled waveguide structure. As depicted in Fig. 4(a), the original resonance peak in Fig. 3 is split, and a narrower dip comes into being at the original

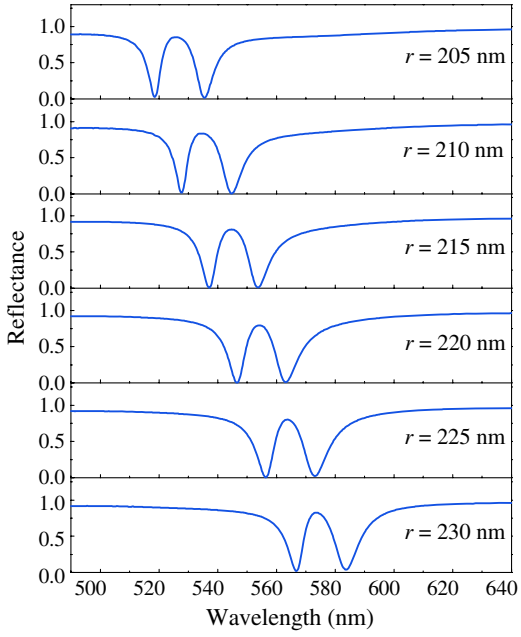

Fig. 3. Reflection spectra with different r in the triple-cavity-coupled waveguide structure with $g = 38$ nm.

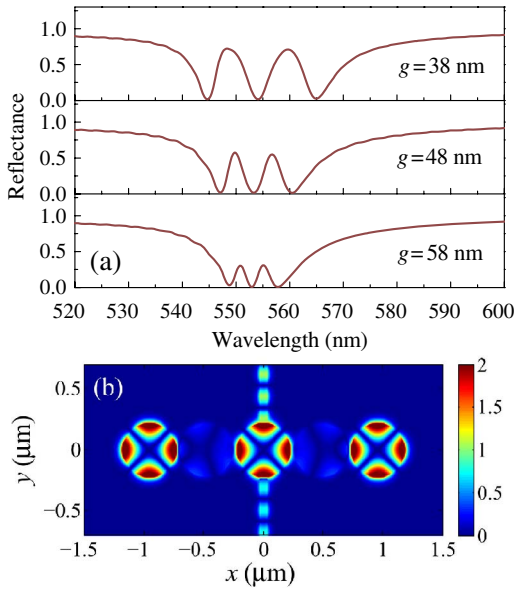

Fig. 4. (a) Reflection spectra with different g in the five-cavity-coupled waveguide structure. (b) Field distribution ($|H_z|$) at the middle dip (554 nm) of the reflection spectrum for $g = 38$ nm (Media 2). Here, r is set as 220 nm.

reflection peak (554 nm) in the five-cavity-coupled waveguide structure. The bandwidth of induced reflection dip also decreases as the coupling distance increases. The corresponding field distribution in Fig. 4(b) shows an interesting phenomenon that the resonance of central and side cavities (i.e., cavity 1, 4, and 5) are excited, while cavity 2 and 3 are off-resonance. The phase-coupled effect, similar to the EIT-like performance, plays an important role in the spectral-splitting processes [44,45]. The physical mechanism can be simply described as follows. The resonance in cavity 4 is established by coupling from cavity 2. The coupling light from cavity 4 to cavity 2 has a π phase shift. Thus, the coupling energies from cavity 1 and 4 result in the destructive interference and hence induce the vanishment of the optical field in cavity 2. Similarly, the destructive interference happens in cavity 3.

In accordance to the above principles, the spectral splitting can be further achieved in the multi-resonator-coupled waveguide systems. For example, the spectral splitting with three reflection peaks is obtained by constructing a symmetrical seven-cavity-coupled waveguide structure. As shown in Fig. 5(a), the middle reflection dip is split, generating an induced-reflection peak. Figure 5(b) describes the field distribution at the middle reflection peak (554 nm). The resonance feature in the waveguide system can be analyzed by the phase-coupled effects as discussed above.

It is not difficult to find that spectral splitting contributes to narrowing the bandwidth of resonance peaks, which benefits improvements of the quality factor. The quality factor of the plasmonic cavity-coupled waveguide can be calculated from $Q = \lambda_0/\Delta\lambda$, where λ_0 and $\Delta\lambda$ are the central wavelength and full-width at half-maximum of the reflection

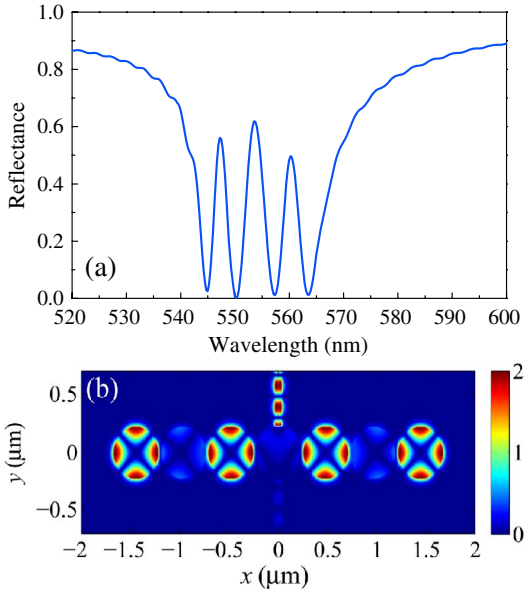

Fig. 5. (a) Reflection spectra in the seven-cavity-coupled waveguide structure. (b) Field distribution ($|H_z|$) at the reflection peak of 554 nm (Media 3). Here, $r = 220$ nm and $g = 38$ nm.

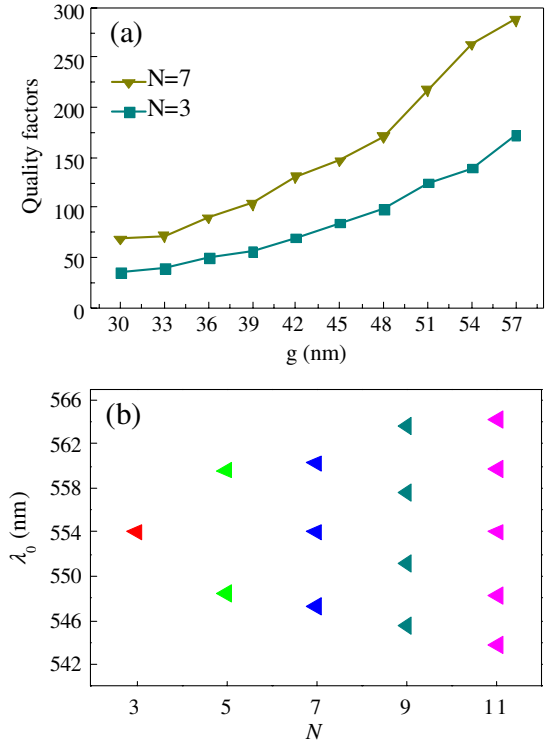

Fig. 6. (a) Quality factors of spectral resonance peaks at the wavelength of 554 nm in the triple- and seven-cavity-coupled waveguide structure with different g. (b) Spectral-splitting evolution as a function of cavity number N. λ_0 represents the wavelength of all reflection peaks.

peak, respectively. Figure 6(a) plots the quality factors of resonance peaks at the wavelength of 554 nm in the triple- and seven-cavity-coupled waveguide structures. It is found that the quality factors are rapidly improved when more cavities are introduced in the plasmonic waveguide system. Moreover, the larger coupling distance leads to a higher-quality factor. As presented in Fig. 6(a), the quality factor of the seven-cavity-coupled structure can approach the level of several hundreds, which is excellent compared with the reported results in [36,37,39]. The evolution of spectral splitting with the cavity number is depicted in Fig. 6(b), exhibiting that a single resonance peak is split into two peaks, and eventually five peaks at the cavity number $N = 11$. That is to say, the splitting of central resonance results in the generation of multiple reflection peaks, which can be used to design multichannel bandpass plasmonic filters [41]. With the excellent resonance performance of multiwavelength and high-quality factors, the proposed plasmonic waveguide systems also may find potential applications for low-threshold optical switching [28,29]. On the other hand, due to the high group-index characteristic of the EIT-like window, slow-light devices can be constructed based on the proposed systems [33,34].

4. Conclusion

Spectral-splitting behaviors have been investigated numerically in multi-resonator-coupled plasmonic

waveguide systems by the FDTD simulations for the first time. We find that a plasmon-induced peak is generated in the reflection dip when another identical cavity is introduced to couple with the central cavity in the plasmonic structure. The results can be exactly explained by the analogue of EIT effects. The symmetrical cavity-coupled structure possesses more obvious spectral-splitting peaks, which can be tuned by the radius of the disk cavity. By cascading multiple cavities into the waveguide system, the reflection spectra can be effectively split. Moreover, the quality factor of the resonance spectrum exhibits an excellent enhancement with the increase of cavity number. The considerable spectral features may pave a pathway toward optical control in the plasmonic waveguide systems and have potential applications for highly integrated optical devices, such as multichannel filters, optical switches, and so on.

This work was supported by the National Natural Science Foundation of China under grants 61223007 and 11204368.

References

1. W. L. Barnes, A. Dereux, and T. W. Ebbesen, "Surface plasmon subwavelength optics," Nature **424**, 824–830 (2003).
2. S. I. Bozhevolnyi, V. S. Volkov, E. Devaux, J. Y. Laluet, and T. W. Ebbesen, "Channel plasmon subwavelength waveguide components including interferometers and ring resonators," Nature **440**, 508–511 (2006).
3. Q. Gan, Y. Gao, K. Wagner, D. Vezenov, Y. J. Ding, and F. J. Bartoli, "Experimental verification of the rainbow trapping effect in adiabatic plasmonic gratings," Proc. Natl. Acad. Sci. USA **108**, 5169–5173 (2011).
4. H. Lu, X. M. Liu, D. Mao, and G. X. Wang, "Plasmonic nanosensor based on Fano resonance in waveguide-coupled resonators," Opt. Lett. **37**, 3780–3782 (2012).
5. R. Zhou, H. Lu, X. Liu, Y. Gong, and D. Mao, "Second-harmonic generation from a periodic array of noncentrosymmetric nanoholes," J. Opt. Soc. Am. B **27**, 2405–2409 (2010).
6. H. Lu, X. Liu, R. Zhou, Y. Gong, and D. Mao, "Second-harmonic generation from metal-film nanohole arrays," Appl. Opt. **49**, 2347–2351 (2010).
7. J. Park, K. Y. Kim, I. M. Lee, H. Na, S. Y. Lee, and B. Lee, "Trapping light in plasmonic waveguides," Opt. Express **18**, 598–623 (2010).
8. H. Lu, X. M. Liu, Y. K. Gong, D. Mao, and L. R. Wang, "Optical bistability in metal-insulator-metal plasmonic Bragg waveguides with Kerr nonlinear defects," Appl. Opt. **50**, 1307–1311 (2011).
9. G. Wang, H. Lu, and X. Liu, "Trapping of surface plasmon waves in graded grating waveguide system," Appl. Phys. Lett. **101**, 013111 (2012).
10. G. Wang, H. Lu, and X. Liu, "Gain-assisted trapping of light in tapered plasmonic waveguide," Opt. Lett. **38**, 558–560 (2013).
11. N. Verellen, Y. Sonnefraud, H. Sobhani, F. Hao, V. V. Moshchalkov, P. Van Dorpe, P. Nordlander, and S. A. Maier, "Fano resonances in individual coherent plasmonic nanocavities," Nano Lett. **9**, 1663–1667 (2009).
12. J. Chen, Z. Li, S. Yue, J. Xiao, and Q. Gong, "Plasmon-induced transparency in asymmetric T-shape single slit," Nano Lett. **12**, 2494–2498 (2012).
13. Y. K. Gong, L. R. Wang, X. H. Hu, X. H. Li, and X. M. Liu, "Broad-bandgap and low-sidelobe surface plasmon polariton reflector with Bragg-grating-based MIM waveguide," Opt. Express **17**, 13727–13736 (2009).
14. B. Wang and G. P. Wang, "Plasmon Bragg reflectors and nanocavities on flat metallic surfaces," Appl. Phys. Lett. **87**, 013107 (2005).
15. F. F. Hu, H. X. Yi, and Z. P. Zhou, "Wavelength demultiplexing structure based on arrayed plasmonic slot cavities," Opt. Lett. **36**, 1500–1502 (2011).
16. H. Lu, X. Liu, Y. Gong, D. Mao, and L. Wang, "Enhancement of transmission efficiency of nanoplasmonic wavelength demultiplexer based on channel drop filters and reflection nanocavities," Opt. Express **19**, 12885–12890 (2011).
17. G. X. Wang, H. Lu, X. M. Liu, D. Mao, and L. N. Duan, "Tunable multi-channel wavelength demultiplexer based on MIM plasmonic nanodisk resonators at telecommunication regime," Opt. Express **19**, 3513–3518 (2011).
18. H. Lu, X. Liu, L. Wang, D. Mao, and Y. Gong, "Nanoplasmonic triple-wavelength demultiplexers in two-dimensional metallic waveguides," Appl. Phys. B **103**, 877–881 (2011).
19. Z. H. Han, E. Forsberg, and S. L. He, "Surface plasmon Bragg gratings formed in metal-insulator-metal waveguides," IEEE Photon. Technol. Lett. **19**, 91–93 (2007).
20. Y. Gong, X. Liu, H. Lu, L. Wang, and G. Wang, "Perfect absorber supported by optical Tamm states in plasmonic waveguide," Opt. Express **19**, 18393–18398 (2011).
21. G. Veronis and S. Fan, "Theoretical investigation of compact couplers between dielectric slab waveguides and two-dimensional metal-dielectric-metal plasmonic waveguides," Opt. Express **15**, 1211–1221 (2007).
22. H. Lu, X. Liu, G. Wang, and D. Mao, "Tunable high-channel-count bandpass plasmonic filters based on an analogue of electromagnetically induced transparency," Nanotechnology **23**, 444003 (2012).
23. Y. K. Gong, X. M. Liu, and L. R. Wang, "High channel-count plasmonic filter with the metal-insulator-metal Fibonacci-sequence gratings," Opt. Lett. **35**, 285–287 (2010).
24. X. S. Lin and X. G. Huang, "Tooth-shaped plasmonic waveguide filters with nanometeric sizes," Opt. Lett. **33**, 2874–2876 (2008).
25. H. Lu, X. M. Liu, D. Mao, L. R. Wang, and Y. K. Gong, "Tunable band-pass plasmonic waveguide filters with nanodisk resonators," Opt. Express **18**, 17922–17927 (2010).
26. H. Lu, X. Liu, Y. Gong, L. Wang, and D. Mao, "Multi-channel plasmonic waveguide filters with disk-shaped nanocavities," Opt. Commun. **284**, 2613–2616 (2011).
27. Y. K. Gong, Z. Y. Li, J. X. Fu, Y. H. Chen, G. X. Wang, H. Lu, L. R. Wang, and X. M. Liu, "Highly flexible all-optical metamaterial absorption switching assisted by Kerr-nonlinear effect," Opt. Express **19**, 10193–10198 (2011).
28. G. Wang, H. Lu, X. Liu, and Y. Gong, "Numerical investigation of an all-optical switch in a graded nonlinear plasmonic grating," Nanotechnology **23**, 444009 (2012).
29. G. Wang, H. Lu, X. Liu, Y. Gong, and L. Wang, "Optical bistability in metal-insulator-metal plasmonic waveguide with nanodisk resonator containing Kerr nonlinear medium," Appl. Opt. **50**, 5287–5290 (2011).
30. H. Lu, X. Liu, L. Wang, Y. Gong, and D. Mao, "Ultrafast all-optical switching in nanoplasmonic waveguide with Kerr nonlinear resonator," Opt. Express **19**, 2910–2915 (2011).
31. W. Chen, D. C. Abeysinghe, R. L. Nelson, and Q. Zhan, "Plasmonic lens made of multiple concentric metallic rings under radially polarized illumination," Nano Lett. **9**, 4320–4325 (2009).
32. K. J. Boller, A. Imamolu, and S. E. Harris, "Observation of electromagnetically induced transparency," Phys. Rev. Lett. **66**, 2593–2596 (1991).
33. Y. Huang, C. Min, and G. Veronis, "Subwavelength slow-light waveguide based on a plasmonic analogue of electromagnetically induced transparency," Appl. Phys. Lett. **99**, 143117 (2011).
34. G. Wang, H. Lu, and X. Liu, "Dispersionless slow light in MIM waveguide based on a plasmonic analogue of electromagnetically induced transparency," Opt. Express **20**, 20902–20907 (2012).
35. N. Liu, T. Weiss, M. Mesch, L. Langguth, U. Eigenthaler, M. Hirscher, C. Sönnichsen, and H. Giessen, "Planar metamaterial analogue of electromagnetically induced transparency for plasmonic sensing," Nano Lett. **10**, 1103–1107 (2010).

36. H. Lu, X. Liu, and D. Mao, "Plasmonic analog of electromagnetically induced transparency in multi-nanoresonator-coupled waveguide systems," Phys. Rev. A **85**, 053803 (2012).
37. H. Lu, G. Wang, and X. Liu, "Manipulation of light in MIM plasmonic waveguide systems," Chinese Sci. Bull. **58**, 3607–3616 (2013).
38. Q. Xu, S. Sandhu, M. L. Povinelli, J. Shakya, S. Fan, and M. Lipson, "Experimental realization of an on-chip all-optical analogue to electromagnetically induced transparency," Phys. Rev. Lett. **96**, 123901 (2006).
39. H. Lu, X. Liu, D. Mao, Y. Gong, and G. Wang, "Induced transparency in nanoscale plasmonic resonator systems," Opt. Lett. **36**, 3233–3235 (2011).
40. H. Lu and X. M. Liu, "Optical bistability in subwavelength compound metallic grating," Opt. Express **21**, 13794–13799 (2013).
41. J. Chen, C. Wang, R. Zhang, and J. Xiao, "Multiple plasmon-induced transparencies in coupled-resonator systems," Opt. Lett. **37**, 5133–5135 (2012).
42. H. L. Liu, B. Li, L. J. Zheng, C. Xu, G. B. Zhang, X. J. Wu, and N. Xiang, "Multispectral plasmon-induced transparency in triangle and nanorod(s) hybrid nanostructures," Opt. Lett. **38**, 977–979 (2013).
43. H. Lu, X. Liu, D. Mao, Y. Gong, and G. Wang, "Analysis of nanoplasmonic wavelength demultiplexing based on MIM waveguides," J. Opt. Soc. Am. B **28**, 1616–1621 (2011).
44. R. D. Kekatpure, E. S. Barnard, W. Cai, and M. L. Brongersma, "Phase-coupled plasmon induced transparency," Phys. Rev. Lett. **104**, 243902 (2010).
45. A. Artar, A. Yanik, and H. Altug, "Multispectral plasmon induced transparency in coupled meta-atoms," Nano Lett. **11**, 1685–1689 (2011).